Evaluation of geometrical contributions to the spread of the Compton-scatter energy distribution

A. L. Hanson
Brookhaven National Laboratory, Upton, New York 11973

G. E. Gigante
Dipartimento di Fisica, Università degli Studi di Roma I, "La Sapienza," Corso Vittorio Emanuele II, 244, 00186 Roma, Italy

(Received 28 December 1988)

The spectrum from Compton-scattered x rays is an inherently broad distribution. This distribution is the sum of several Gaussian-like distributions, which gives the sum its unique shape. The Gaussian-like distributions are the result of convoluting the so-called Compton profile, the spread in the scattered-x-ray energies due to the momentum distributions of the target electrons, with the detector response and the geometrical effects. The distribution is then further modified by the absorption within the sample. A formulation for both qualitatively and quantitatively determining the magnitude of the geometrical contributions is presented. This formulation is based on a recently devised approach to the scattering geometry [Hanson, Gigante, Meron, Phys. Rev. Lett. **61**, 135 (1988)]. A methodology for determining the geometrical spread in the energy of the scattered x rays is presented. The results can be conveniently used to optimize scattering geometries for the reduction of the geometry-caused spread.

I. INTRODUCTION

Compton-scattered x-rays have been used as probes for the measurements of several physical quantities such as electron density, target mass, and mass density.[1,2] When used with coherently scattered x-rays it has also been used for Z-dependent characterization of materials.[3,4] The width of the Compton distribution is inherently broad which is an obstacle in the analytical measurements that relate the total Compton intensity to the quantity of interest. In fact, the Compton scattering results not in a peak, but in a non-Gaussian distribution of x-ray energies. For many spectrometric techniques, such as x-ray fluorescence (XRF), the Compton scattering can be the largest direct or indirect source of background. Moreover, with the advent of electron synchrotron storage rings as x-ray sources, the use of tunable, monochromatic radiation for sophisticated physical analyses leads to more restrictive requirements on the background evaluation. This is especially true when the incident x-ray energy is just above the absorption edge of the element being probed. In particular, in XRF with monochromated synchrotron radiation the Compton-scattered x-rays result in a high background in the spectral energy region just below the primary radiation.[5] Therefore the incident energy must be set relatively far from the edge of the element being analyzed. Some authors have regretted the fact that the level of scattering is higher than originally anticipated and is the cause for not achieving the previously predicted ultimate minimum detectable limits (MDL's), measured with energy-dispersive spectrometers (EDS's), for the analysis of any particular element. In light of this, the measurements of chemical speciation, measurement of shifts in the photoelectric absorption edge as the incident x-ray energy is scanned, will be hampered by the presence of the Compton-scattered x-rays. There are numerous other x-ray-based techniques where the scattered x rays, and other effects such as x-ray resonant Raman scattering, must be accurately removed from the spectra. Finally, along this line, knowledge of the shape of the Compton distribution is important for accurate measurements of the Compton cross section.

For some authors the inherent width of the Compton-scattered x-ray distribution is utilized for determining the electron-momentum distributions of elements, known as the Compton profile.[6,7] Unfortunately, the energy distribution of the Compton-scattered photons is due only in part to the electron-momentum distribution. The width and shape of the measured distribution also includes detector-response, geometrical, and absorption contributions that are not negligible. The only way to avoid geometrical effects is to use very tight collimation of the beam and the detector. This limits the counting statistics of a particular measurement. Therefore any Compton-scattering measurement requires a tradeoff between the need to increase the counting statistics and the spread of the Compton-scatter distribution. The relative magnitude of the geometrical contribution depends on the resolution of the detector. In order to optimize the design of a Compton spectrometer, many parameters must be adjusted, such as the energy of the primary beam and the scattering angle.

In general, we can stress that the choice of the x-ray energy is more related to x-ray absorption, whereas that of the scattering angle is more related to the geometry. Only a few authors have attempted to include geometri-

cal spread in the optimization procedures and data analysis.[6–9] The evaluation of all of these contributions is mandatory in Compton-profile measurements and is important in other spectroscopic techniques in order to achieve good results.

The distribution of Compton-scattered x-rays is a sum of energy distributions resulting from the scattering of the primary photons by electrons in each orbital. For the most tightly bound electrons the uncertainty in the electron momentum, Δp, results in an extremely broad component of the scatter distribution. The outer-shell electrons are responsible for the central peak of the distribution. Ignoring absorption effects, the distribution of scattered energies is always centered about the most probable energy E, which is related to the incident energy E_0 and to the scattering angle θ by

$$\frac{E}{E_0}=\frac{1}{1+\gamma[1-\cos(\theta)]}\ , \tag{1}$$

where $\gamma=E_0/m_0c^2$. The energy distribution of the Compton-scattered x rays about the mean energy E can be calculated according to methods presented by Carlsson *et al.*[10] and by Ribberfors and Berggren.[11] Equation (1) illustrates that there is an angular dependence on the energy of the scattered x-rays. If the interaction volume is large enough to create a significant $\Delta\theta$, then there is a spread in the measured scattered energy distribution due to the geometrical effects. Each dimension of the sample can contribute to this spread in $\Delta\theta$. From here on in this paper E/E_0 and $\Delta E/E_0$ will be represented with $\bar{E}$ and $\Delta\bar{E}$.

In this work we have determined independently and analytically the contributions of the geometrical effects that result in a spread ($\Delta\bar{E}$) of the Compton-scatter distribution. This geometry-caused spread is due to the dependence of the scattered energy on the scattering angle. In a previous work we presented a reference system that simplifies the derivation of the isoscattering contours. In this work we utilize these contours to relate measuring-system parameters to the geometry-caused energy spread.

II. THEORY

A. Basic (two dimensions)

The aim of this work is to find a relation between the energy spread caused by geometry and the geometrical parameters of the measuring system. The first step is to determine the effective dimensions of the sample with respect to measuring-system parameters, initially neglecting absorption. The basic geometry is shown in Fig. 1(a). It is implied that the detector- and source-defining apertures or slits are normal to and centered on their respective axes. The shape of the intersection region is determined by the scattering angle, the shape of the slits or collimators, and the distances between the source (S) and the sample and detector (D) and the sample. The actual physical dimensions of a nonabsorbing sample is then the intersection between the scatter volume (V) and the sample. Absorption characteristics of the sample will then reduce the effective size of the sample. We will define the effective sample as being represented by a rectangular solid with the sides given by $\Delta\bar{r}(=\Delta r/b)$, $\Delta\bar{z}\ (=\Delta z/b)$, and, out of this plane, $\Delta\bar{h}\ (=\Delta h/b)$. In this way we formalize the problem and in the following will refer to the effective sample as the sample. The intersection between the fields of view of the detector and the source, each of which are conical in shape, is known as the scattering volume (V). The fields of view and their intersection can be visualized with the aid of Fig. 1(b).

The geometrical spread ($\Delta\bar{E}$) is due to the spread in the scattering angle accepted by the sample ($2\Delta\theta$), as determined by Eq. (2a) for small scattering volumes and (2b) for large scattering volumes,

$$\Delta\bar{E}=\frac{d\bar{E}}{d\theta}\Delta\theta\ , \tag{2a}$$

$$\Delta\bar{E}=\int\frac{d\bar{E}}{d\theta}d\theta\ . \tag{2b}$$

A qualitative approach for determining $\Delta\theta$ is to overlay contours of the constant-scattering angle, presented in Ref. 12, over the defined sample. In this way we can

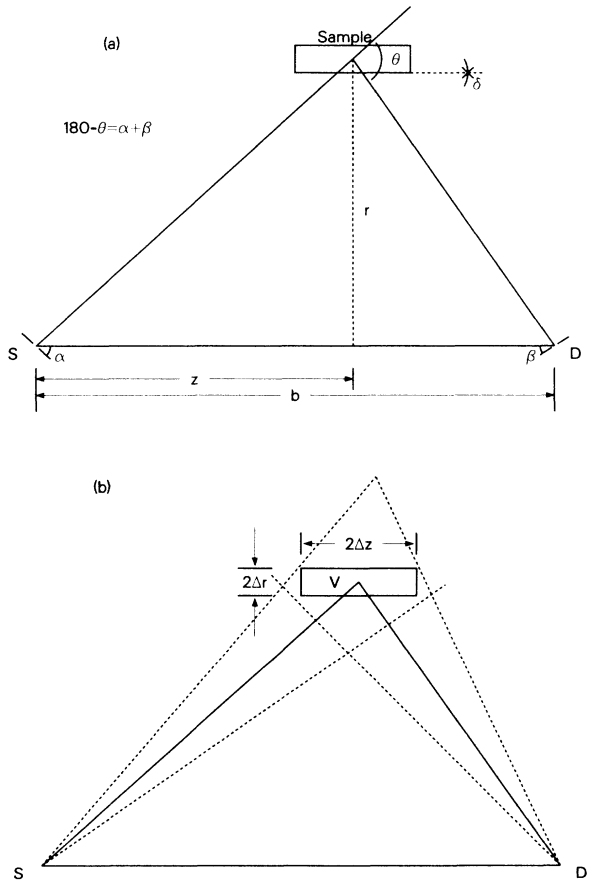

FIG. 1. (a) Basic sample geometry. (b) Sample geometry with field of view of the detector and source included.

visualize $\Delta\theta$ subtended by the sample. Since we are interested in the energy spread $\Delta\bar{E}$ instead of $\Delta\theta$, a more appropriate approach for determining $\Delta\bar{E}$ is to perform this visualization with contours of constant-scattered energy. From Eq. (1) there is a 1:1 correlation between energy and θ which provides us with a starting point for understanding problem of spread of the scattered energy distribution resulting from the geometry of the system.

The contours of constant scattered energy that correspond to the contours of the constant scattering angle, as a function of $\bar{r}$ ($=r/b$) and $\bar{z}$ ($=z/b$), are shown in Fig. 2 for incident x-ray (or γ-ray) energies of 17.5, 60, 160, 412, and 662 keV, probe energies commonly reported in the literature. From these plots it can be noted that the gradients in the scattered energy become steeper as the incident energy is increased. The contours of the constant scattering angle, as a function of $\bar{r}$ and $\bar{z}$, were determined with Eq. (3) and the contours of the constant scattering energy were determined by substituting θ from Eq. (3) (Ref. 12) into Eq. (1),

$$\tan(\theta)=\frac{\bar{r}}{\bar{z}(1-\bar{z})-\bar{r}^2} . \tag{3}$$

These contours are toroidal in nature with *S-D* as the axis of symmetry. Therefore the approach that we will follow to discuss the problem in the *R-Z* plane and later generalize the results to include the third dimension. The previous presentation of isoenergy contours are extremely effective in the definition of the problem, but does not allow for an analytical determination of the energy spread. Therefore our goal is to determine the gradients in energy subtended by the sample as a function of the sample's spatial coordinates for a given $\Delta\bar{r}$ and $\Delta\bar{z}$, i.e., the sample.

Since the *R* and *Z* axes are Cartesian, we can easily describe two of the three dimensions of the sample in $\bar{r}$ and $\bar{z}$. With this approach we can describe θ in terms of $\bar{r}$ and $\bar{z}$ and the dimensions of the sample and scattering volume in terms of $\Delta\bar{r}$ and $\Delta\bar{z}$ instead of $\Delta\theta$. $\Delta\bar{E}$ can then be calculated with

$$\Delta\bar{E}=C_1\Delta\bar{r}+\frac{C_2}{2}\Delta\bar{r}^2+C_3\Delta\bar{z}+\frac{C_4}{2}\Delta\bar{z}^2+C_5\Delta\bar{r}\,\Delta\bar{z} , \tag{4}$$

where

$$C_1=\left|\frac{d\bar{E}}{d\bar{r}}\right| ,$$

$$C_2=\left|\frac{d^2\bar{E}}{d\bar{r}^2}\right| ,$$

$$C_3=\left|\frac{d\bar{E}}{d\bar{z}}\right| ,$$

$$C_4=\left|\frac{d^2\bar{E}}{d\bar{z}^2}\right| ,$$

$$C_5=\left|\frac{d^2\bar{E}}{d\bar{r}\,d\bar{z}}\right| .$$

In order to define our derivatives, it is convenient to make the definitions

$$s=\tan(\theta) ,$$

$$w=1-2\bar{z} ,$$

$$x=(s^2+1)^{1/2} ,$$

$$u=\gamma(1-1/x)+1 ,$$

$$a=\bar{z}(1-\bar{z}) ,$$

$$y=2\bar{r}s+1=\frac{a+\bar{r}^2}{a-\bar{r}^2} .$$

The appropriate differentials are

$$\frac{d\bar{E}}{d\bar{r}}=-\frac{\gamma s^2 y}{x^3\bar{r}u^2} ,$$

$$\frac{d^2\bar{E}}{d\bar{r}^2}=\frac{\gamma s^2[2\gamma s^2y^2-xu(3y^2-x^2y-x^2)]}{x^6\bar{r}^2u^3} ,$$

$$\frac{d\bar{E}}{d\bar{z}}=\frac{\gamma s^3 w}{x^3\bar{r}u^2} ,$$

$$\frac{d^2\bar{E}}{d\bar{z}^2}=\frac{-3\gamma s^4xuw^2+2\gamma^2s^6w^2-2\gamma s^3x^3\bar{r}u}{x^6\bar{r}^2u^3} ,$$

$$\frac{d^2\bar{E}}{d\bar{r}\,d\bar{z}}=\frac{\gamma s^3w[xu(3y-x^2)-2\gamma s^2y]}{x^6\bar{r}^2u^3} .$$

As will be shown later, the higher-order derivatives are needed since $d\bar{E}/d\bar{z}$ is zero at $\bar{z}=0.5$. The coefficients use absolute values since the derivatives change sign. It is interesting to note that there is a singularity at $\bar{r}^2=\bar{z}(1-\bar{z})$, or $\theta=90°$. Therefore at 90° we need to take the limit as $s\rightarrow\infty$,

$$\frac{d\bar{E}}{d\bar{r}}=-\frac{2\gamma}{(\gamma+1)^2} ,$$

$$\frac{d^2\bar{E}}{d\bar{r}^2}=\frac{2\gamma(4\gamma\bar{r}+\gamma+1)}{(\gamma+1)^3\bar{r}} ,$$

$$\frac{d\bar{E}}{d\bar{z}}=\frac{\gamma w}{(\gamma+1)^2\bar{r}} ,$$

$$\frac{d^2\bar{E}}{d\bar{z}^2}=\frac{2\gamma(\gamma w^2-\gamma\bar{r}-\bar{r})}{(\gamma+1)^3\bar{r}^2} ,$$

$$\frac{d^2\bar{E}}{d\bar{r}\,d\bar{z}}=-\frac{\gamma(4\gamma\bar{r}+\gamma+1)w}{(\gamma+1)^3\bar{r}^2} .$$

Equation (5) gives $\Delta\bar{E}$ as a function of spatial coordinates for a small sample. If the dimensions of the sample become too large, then Eq. (5) must be integrated with respect to $\bar{r}$ and $\bar{z}$. If the sample has been placed so that the coefficients, i.e., the derivatives, are slowing varying functions of $\bar{r}$ and $\bar{z}$, then the coefficients can be considered constant over the integration. In this way a nonrectangular shaped sample can be described and the integration over the sample can be simplified. This concept is important in that the sample can be divided into segments, later to be reconstructed, and the attenuation can be included.

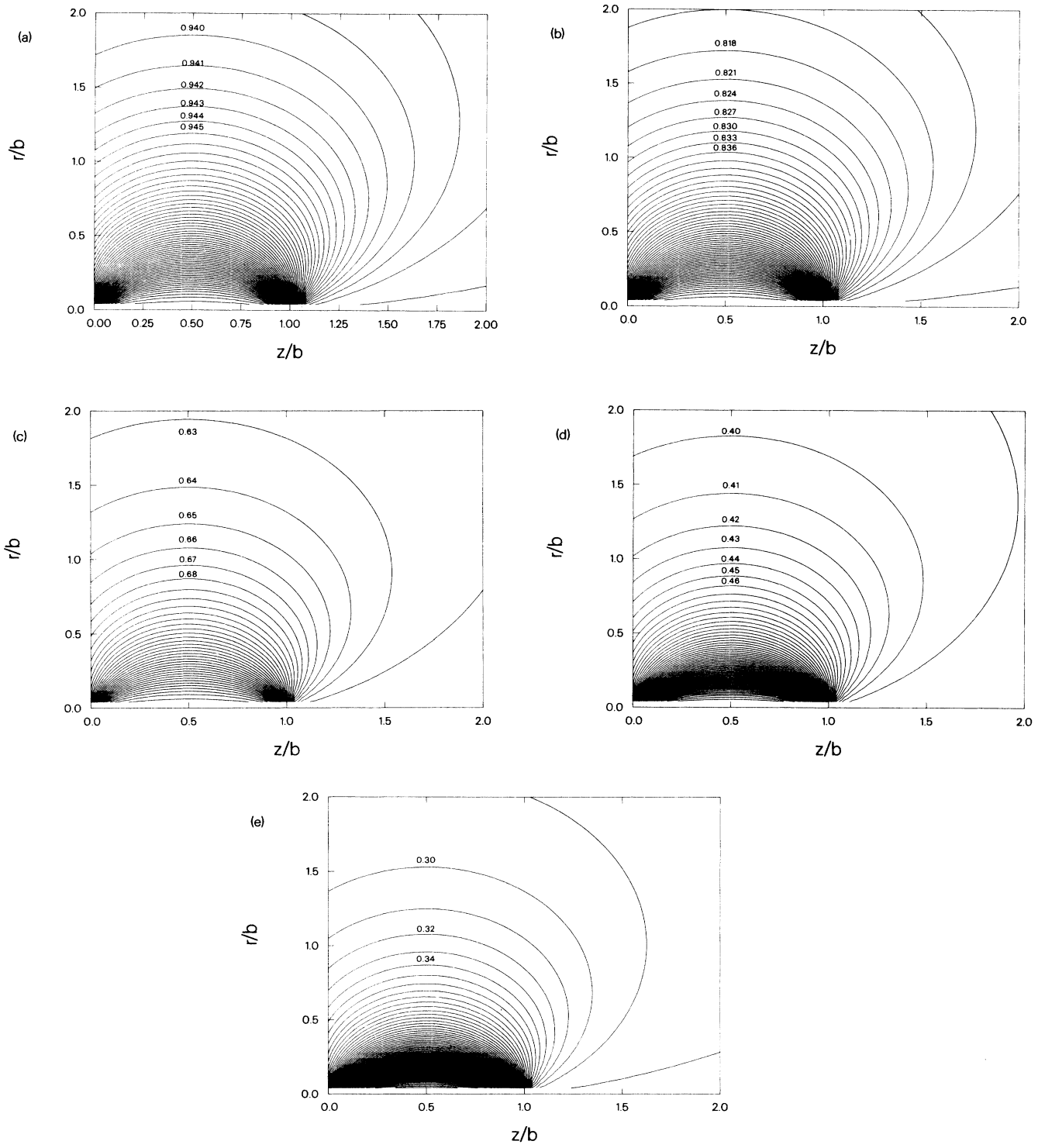

FIG. 2. (a) Contours of constant scattering energy for an incident energy of 17.5 keV. The labels on the contours are the ratios of scattered-to-incident x-ray energy. (b) Contours of constant-scattering energy for an incident energy of 60 keV. The labels on the contours are the ratios of scattered-to-incident x-ray energy. (c) Contours of constant-scattering energy for an incident energy of 160 keV. The labels on the contours are the ratios of scattered-to-incident x-ray energy. (d) Contours of constant scattering energy for an incident energy of 412 keV. The labels on the contours are the ratios of scattered-to-incident x-ray energy. (e) Contours of constant scattering energy for an incident energy 662 keV. The labels on the contours are the ratios of scattered-to-incident x-ray energy.

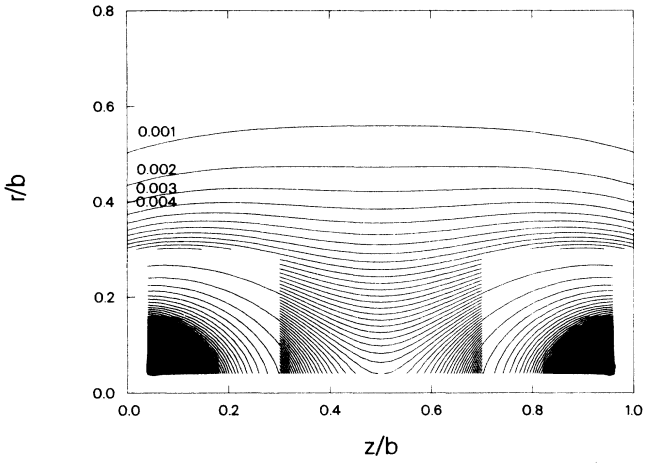

FIG 3. Contours of isoefficiency assuming a point-scattering volume. the labels are for values of ϵ as calculated by Eq. (5).

B. Contours of constant efficiency

In order to determine the most appropriate geometry for a given measurement, we must balance the geometrical spread that we are willing to accept with the efficiency of detection that we are willing to lose. For an isotropic source, if A_s and A_d are the areas of the source and detector apertures, respectively, we can write a relation for the efficiency of the system as

$$\epsilon = \left[\frac{A_s}{\bar{r}^2+\bar{z}^2}\right]\left[\frac{A_d}{\bar{r}^2+(1-\bar{z})^2}\right] . \quad (5)$$

Figure 3 shows a contour plot of isoefficiency as a function of $\bar{r}$ and $\bar{z}$ for source and detector areas, normalized to b^2, of 0.01. The equation for the efficiency is for a point of scatter and neglects the lateral response function for points off the detector and source axes. This approximation is reasonable for assessing the magnitude of changes in efficiency as the sample position is moved, but a more sophisticated version of efficiency is needed for quantitative analyses.

C. The third dimension

We need to include a method to determine the spread resulting from the third dimension, $\Delta\bar{h}$, of any real sample. As was shown in Refs. 12 and 13, we have azimuthal symmetry about the source-detector axis. Hence the three-dimensional surfaces of constant scattering angle and contours of constant scattering energy are toroidal in shape. By invoking this symmetry, the third dimension of the sample can be dealt with by projecting points off the R-Z plane along the toroidal surface to the R-Z plane. This is illustrated in Fig. 4. For most cases $\delta\bar{h}_1$ is approximately equal to $\delta\bar{h}_2$, so we can define $\bar{r}^1=\bar{r}+\delta\bar{h}$. We can now use the same equations for calculating $\Delta\bar{E}$ in two dimensions by including a set of terms that have $\bar{r}$ replaced with $\bar{r}^1$. This method approximates a sample that is a rectangle in height with one that is a section of two concentric toroids. Unless $\bar{h}/2$ is large, this will be a

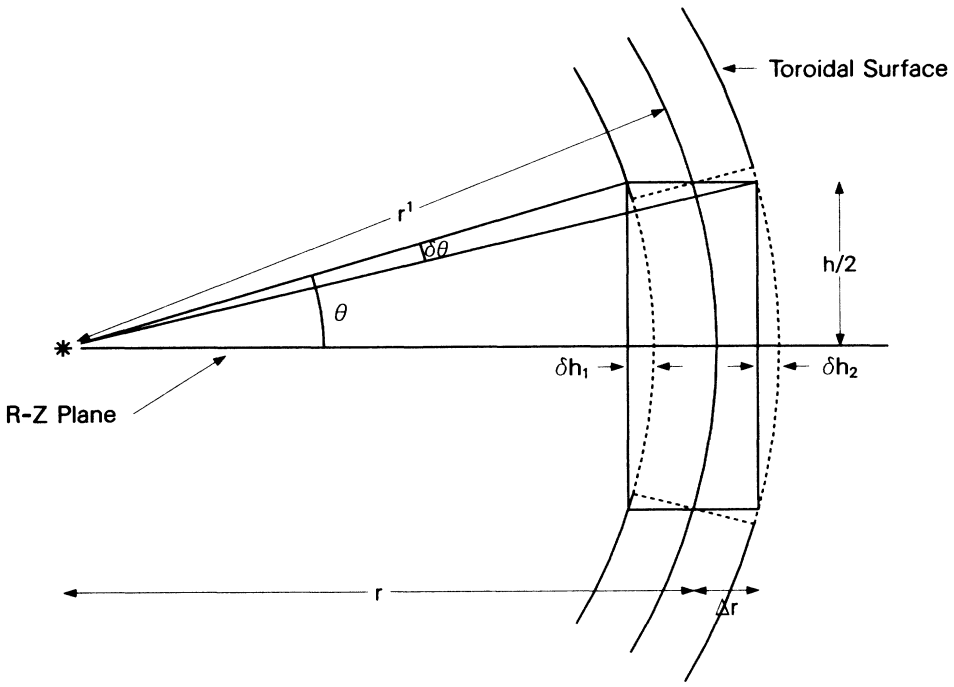

FIG. 4. Projection of sample onto the R-Z plane along the toroidal contour surfaces.

second-order correction to $\bar{r}$.

As a brief aside, it is interesting at this point to consider a sample that is thread or a thin rod with only a significant $\bar{h}$ component. If the rod is placed at θ in the R-Z plane, then this rod is tangential to the θ (toroidal) surface. As the length of the rod is increased, $\Delta\theta$ increases as we cross more surfaces of constant scattering angle. The effective scattering angle of the sample will likewise increase with the length of the rod. The angle θ is now the minimum angle in the distribution of subtended scattering angles and not the mean scattering angle of the rod.

III. RESULTS

The general approach of optimizing the design of a Compton spectrometer requires several tradeoffs. For example, the primary energy is chosen after compromising between the attenuation of the photons by the sample and the detector parameters of efficiency and energy resolution. The scattering angle, $\bar{r}$, and $\bar{z}$ are selected according to the type of information needed and the physical constraints of the measurement system. The angle, energy, and efficiency contours, already presented, are useful in optimizing and understanding the design of a scattering spectrometer when all other experimental constraints that restrict the field of options are taken into account.

From the energy-contour plots we can estimate the energy spread of Compton scattered x-rays by determining the number of contour lines, weighted with the relative length of the segments, that are subtended by the sample. By determining the number of contour lines subtended by the sample, we are actually measuring the gradient of the energy distribution within the sample. In a rapid assessment of the situation, it is then convenient to study the contour plots of the energy spread as a function of $\bar{r}$ and

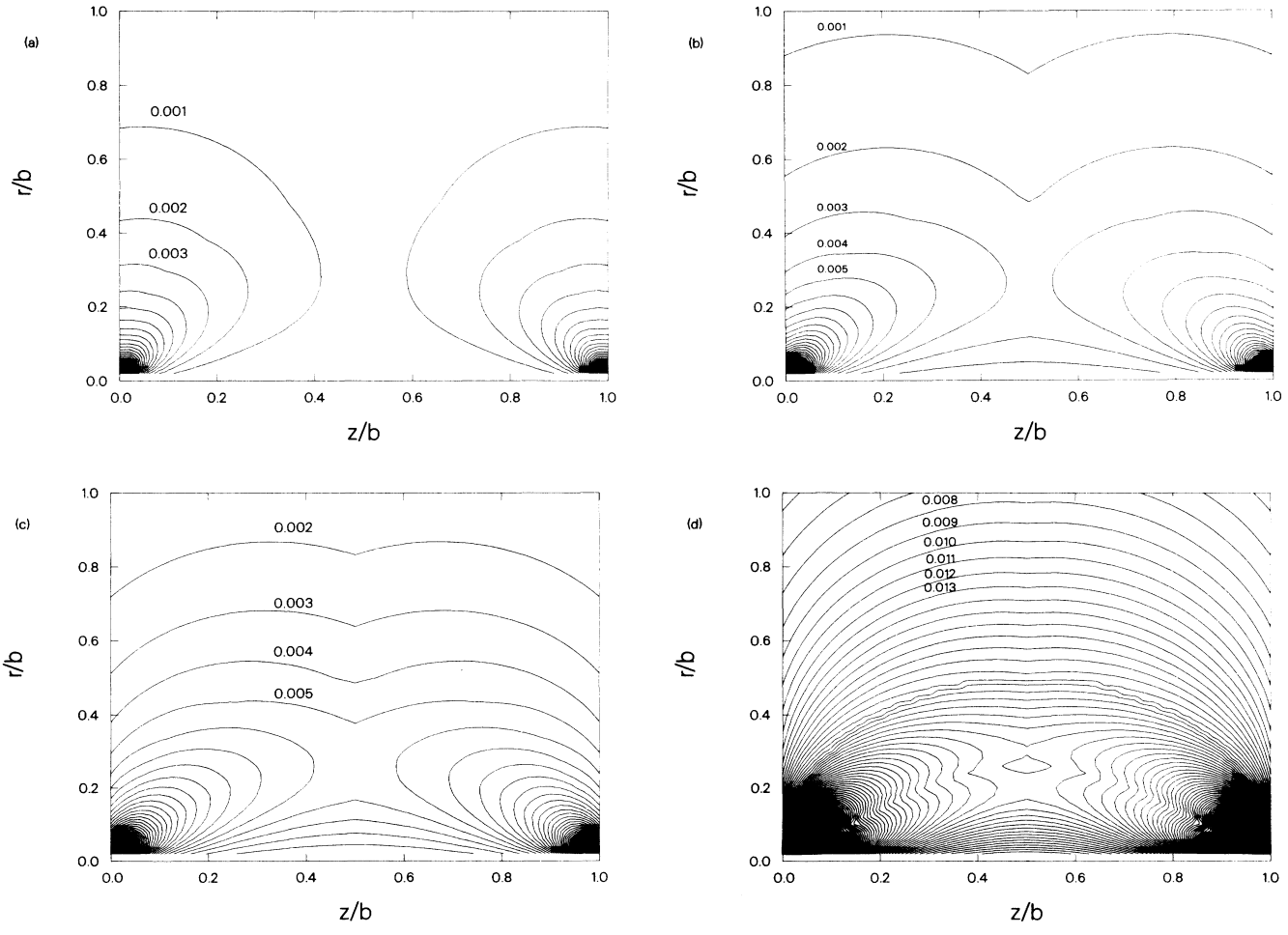

FIG. 5. (a) Contours of constant $\Delta\bar{E}$ for 60-keV incident x rays with $\Delta\bar{r}=0.002$ and $\Delta\bar{z}=0.01$. The labels are actual values of $\Delta\bar{E}$. (b) Contours of constant $\Delta\bar{E}$ for 60-keV incident x rays with $\Delta\bar{r}=0.01$ and $\Delta\bar{z}=0.01$. The labels are actual values of $\Delta\bar{E}$. (c) Contours of constant $\Delta\bar{E}$ for 60-keV incident x-rays with $\Delta\bar{r}=0.02$ and $\Delta\bar{z}=0.01$. The labels are actual values of $\Delta\bar{E}$. (d) Contours of constant $\Delta\bar{E}$ for 60-keV incident x-rays with $\Delta\bar{r}=0.1$ and $\Delta\bar{z}=0.01$. The labels are actual values of $\Delta\bar{E}$.

$\bar{z}$. As an example, we present contour plots of constant $\Delta\bar{E}$ as a function of $\bar{r}$ and $\bar{z}$ in Fig. 5. The curves were generated for a photon energy of 60 keV and $\Delta\bar{r}$ values of 0.002, 0.01, and 0.02 holding $\Delta\bar{z}$ at 0.01. The value of 0.002 for $\Delta\bar{r}$ is equivalent to using a 1-mm-thick sample in the spectrometer of Pattison and Schneider.[7] The value of $\Delta\bar{z}=0.01$ is on the order of the normalized aperture sizes used by Pattison and Schneider. From these plots the gradients are, of course, steepest as $\bar{r}$ approaches zero and less steep as $\bar{r}$ becomes large (implying large θ). The gradient is minimized when $\bar{z}=0.5$, which corresponds to the distance S-V being equal to S-D. As the sample becomes thicker (larger $\Delta\bar{r}$) the gradients within the sample become steeper as the sample subtends more constant energy-contour lines. The gradient minima at $\bar{z}=0.5$ become less pronounced.

When determining $\Delta\bar{E}$, it is important to consider if and when higher-order contributions can be neglected. We therefore present plots of the percentage contribution from the $(d\bar{E}/d\bar{r})\Delta\bar{r}$ and $(d\bar{E}/d\bar{z})\Delta\bar{z}$ terms along with the sum of the higher-order terms. Plots generated for 60-keV photons with $\Delta\bar{r}=0.01$ and $\Delta\bar{z}=0.01$ are presented in Fig. 6 for the scattering into 90° and 165°. At 165°, for all values of $\bar{z}$, the higher-order terms contribute less than 1% even though the $d\bar{E}/d\bar{z}$ is zero at $\bar{z}=0.5$. At 90°, the higher-order terms contribute about 12%. The relative magnitude of each contribution does not change significantly with energy. However, as $\Delta\bar{r}$ and $\Delta\bar{z}$ are increased the higher-order terms become significant. When $\Delta\bar{r}=\Delta\bar{z}=0.1$ the higher-order terms contribute 2–8% at 165° and contribute 20–30 % at 90°. The magnitude of the contributions is symmetrical about 90°.

One aspect of the suggested optimization procedure that has not been addressed until now is the effect that $\Delta\bar{r}$ and $\Delta\bar{z}$ have on $\Delta\bar{E}$. As the sample thickness and interaction volume is increased, we will have a more severe broadening of the energy distribution. Therefore it is interesting to plot $\Delta\bar{E}$ as a function of $\Delta\bar{z}$ or $\Delta\bar{r}$. In all cases the $(d\bar{E}/d\bar{r})\Delta\bar{r}$ terms dominate the $\frac{1}{2}(d^2\bar{E}/d\bar{r}^2)\Delta\bar{r}^2$ terms. Therefore holding $\Delta\bar{z}$ constant, $\Delta\bar{E}$ will be almost a linear function of $\Delta\bar{r}$. This is not the case with the $\Delta\bar{z}$ terms since $d\bar{E}/d\bar{z}$ and $d^2\bar{E}/d\bar{r}\,d\bar{z}$ are both zero at $\bar{z}=0.5$. Figure 7 shows $\Delta\bar{E}$ versus $\Delta\bar{z}$ for 60-keV x-rays scattered into 90° with $\bar{r}=0.5$, $\bar{z}=0.5$, and for five values of $\Delta\bar{r}$. Since $d\bar{E}/d\bar{z}$ and $d^2\bar{E}/d\bar{r}\,d\bar{z}$ are both zero at $\bar{z}=0.5$ regardless of scattering angle, the $\Delta\bar{E}$-versus-$\Delta\bar{z}$ curve will be similar in shape for any scattering angle, but the magnitude of the effect will be less pronounced as we move away from 90°. This is because the $\Delta\bar{r}$ terms have larger contributions as was shown in Fig. 6.

In scattering techniques such as Compton-profile measurements, we usually define the geometry with the scattering angle θ. In XRF, where we usually work with thin samples of finite dimensions, it is common to define the angles Ψ and Φ as illustrated in Fig. 8. The relation between them and θ is $\Phi+\Psi=2\theta$. It can be easily demonstrated that if we want to place the sample along a

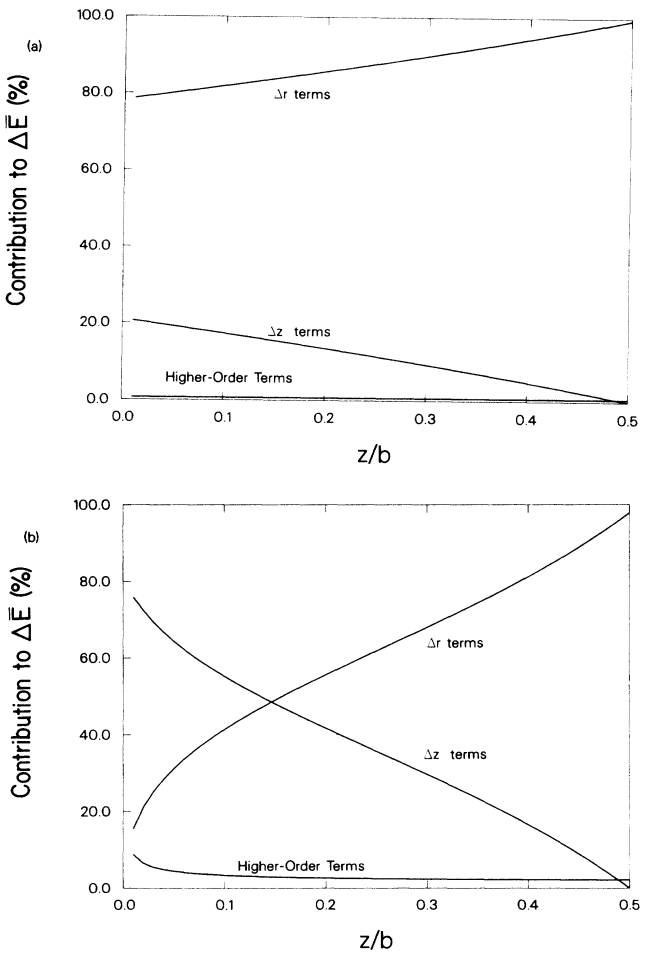

FIG. 6. (a) Percent contribution to $\Delta\bar{E}$, for 60-keV x rays scattered into 165°, of the two first-order terms and the sum of all of the higher-order terms. $\Delta\bar{r}$ and $\Delta\bar{z}$ fixed at 0.01. (b) Percent contribution to $\Delta\bar{E}$, for 60-keV x rays scattered into 90°, from the two first-order terms and the sum of all of the higher-order terms. $\Delta\bar{r}$ and $\Delta\bar{z}$ were fixed at 0.01.

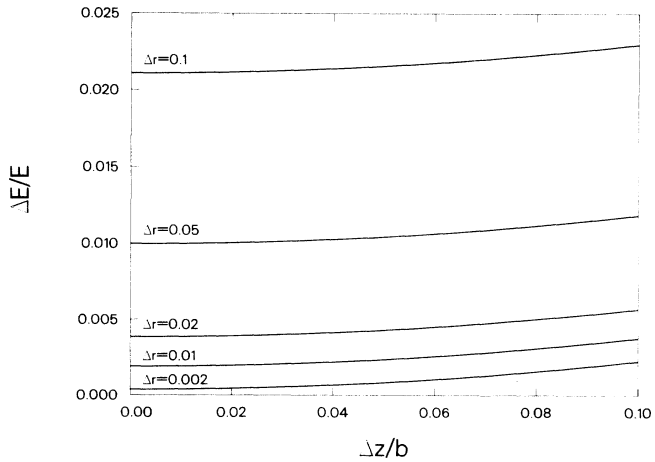

FIG. 7. $\Delta\bar{E}$ vs $\Delta\bar{z}$ for 60-keV x-rays scattered into 90°, for values of $\Delta\bar{r}$ of 0.002, 0.01, 0.02, 0.05, and 0.1. These calculations were for $\bar{r}=\bar{z}=0.5$.

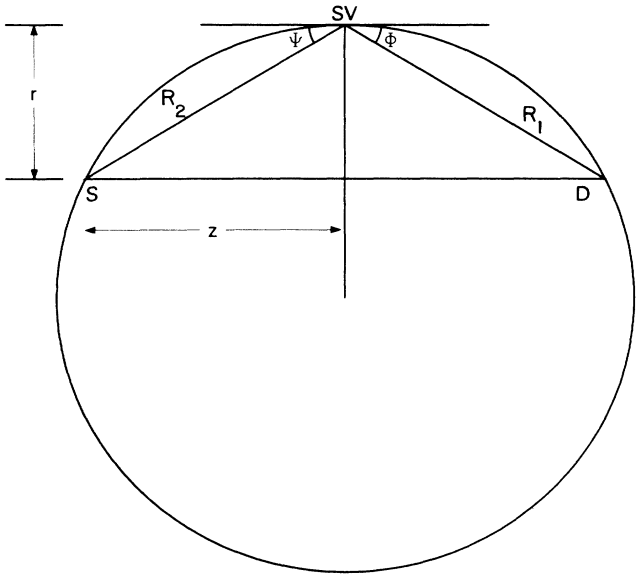

FIG. 8. Correlation between commonly defined XRF geometry and our geometry.

specific contour, we should satisfy the following relation:

$$\frac{\sin\Psi}{\sin\Phi}=\frac{R_1}{R_2}\ . \tag{6}$$

It is worth noting that this simple criterion can be easily implemented in an experimental setup just looking at the distances of the source to detector relative to the target. In addition, we can consider a sample moving along a contour simply when R_1 and/or R_2 are changed. This can be achieved by changing the position of the source and/or the detector along their respective axes. This, in turn, changes $\bar{r}$ and $\bar{z}$, but not necessarily r, z, and b. Therefore by fixing θ we only have one independent variable, either $\bar{r}$ or $\bar{z}$, so a plot of $\Delta\bar{E}$ versus $\bar{r}$ or $\bar{z}$ illustrates the effect of moving the sample along the contour. A set

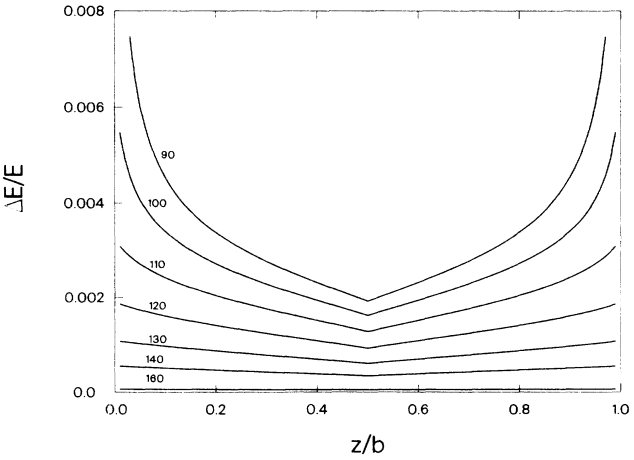

FIG. 9. $\Delta\bar{E}$ as a function of $\bar{z}$ fixing several angles and maintaining a constant b as R_1 and R_2 are changed.

of curves illustrating this is presented in Fig. 9. These curves were generated keeping b constant, which means R_1 and R_2 must be adjusted to maintain the same scattering angle. If only R_1 or R_2 are changed even though θ is constant, b will change along with $\Delta\bar{r}$ and $\Delta\bar{z}$. The curves of Fig. 9 are symmetric about 90°. From these curves it is apparent that in order to minimize $\Delta\bar{E}$ we want $\bar{z}=0.5$ regardless of the scattering angle, even though the fluctuations are minimized in the forward or backward directions. The reason for the changes in $\Delta\bar{E}$ is due to the fluctuations in the relative contributions of the $\Delta\bar{z}$ components illustrated in Fig. 7. The discontinuity at $\bar{z}=0.5$ is from the fact that the derivatives change sign there.

IV. DISCUSSION

The spectrum from Compton-scattered x rays shows an inherently broad and asymmetric distribution. The unique shape of the distribution results from several contributions, such as (a) geometrical, (b) absorption, (c) multiple events, and, last but not least, (d) the natural asymmetry of the Compton profile. The evaluation of each individual contribution has generally been thought to be somewhat difficult, resulting in the large use of Monte Carlo methods for the prediction of Compton spectra.[14] These methods are now quite simple, but they are more helpful in the final evaluation of a measuring system than in the optimization of the system.

The idea to evaluate individually the contributions of the enlargement of the Compton spectra is not new. However, a more specific and analytical approach was needed, especially when the $\Delta\theta$ subtended by the sample becomes large. The problem posed here assumed that we started with a "good" geometry, a rectangular sample totally subtended by interaction volume. It is also assumed that the collimation of the source and detector was rectangular, so no curvature from the aperture are observed out of the R-Z plane. As samples more realistic in shape are assessed, we need to make sure that we take into account the fact that sample dimensions may no be parallel to the R, Z, and H axes. Likewise, when assessing the effects from using a circular aperture we cannot necessarily use the radius of the aperture as $\Delta\bar{z}$ without overestimating $\Delta\bar{E}$. Also, for circular apertures the cone-shaped detector and/or source field of view will be ellipsoidal instead of circular. If the surface of the sample is not parallel to the source-detector axis, then $\Delta\bar{r}$ is not actually the thickness of the sample, but the thickness divided by $\cos(\delta)$, referring back to Fig. 1(a). A similar correction to $\Delta\bar{z}$ will be needed.

In the determination of Compton profiles, if the samples are compared to experimentally determined reference profiles, then as long as the absorption and sample thickness are the same, the geometrical effects and the effects of detector resolution will be a constant contribution of each spectra (i.e., everything washes out). Therefore the work presented here will not be as interesting for the analysis of the spectra as it will be for determining the optimum experimental geometry. However, if the measured spectra are compared to theoretically determined spectra, the geometrical effects and contributions

must be understood. As detector resolution improves, e.g., measuring Compton profiles measured with crystal spectrometers,[15] the requirements for the geometrical effects will become more stringent. As an example, if we imagine a detector resolution of about 200 eV for 60-keV x rays, and we decide to accept 1% or less contribution from the geometrical spread, then this contribution should be less than 28 eV. If we now measure the x rays with a 4-eV detector[15] the maximum acceptable geometrical spread is 1.1 eV, a factor-of-25 reduction in the requirements. In the case of analytical work, especially in medical physics, large samples may be the rule instead of the exception.

In trying to understand the Compton-scatter distribution, we need to realize that the distribution is not a convolution of contributions from each orbital but is a sum of contributions from all orbitals. As such, the effects of detector resolution and geometrical spreading will be convoluted with the contributions from each orbital. That is why even with a relatively poor-energy-resolution detector the entire Compton distribution never tends towards a Gaussian distribution. Since the contribution from each orbital is the convolution of the momentum distribution, the detector resolution, and the geometrical spread, we know from the central-limit theorem that the result will be nearly a Gaussian. If the response function inside the scattering volume is uniform, i.e., each point has equal weight apart from the geometrical spread, the energy distribution from geometrical effects would not be Gaussian in shape. However, there will be an "effective Gaussian" whose sigma is related to our calculated $\Delta\bar{E}$, which when convoluted with our detector response and the Compton profile, will result in an equivalent distribution as before. Therefore, when using the results from this work we must be careful not to use $\Delta\bar{E}$ as the sigma of a Gaussian distribution.

When the subtended $\Delta\theta$ becomes large we may need to integrate Eq. (4) with respect to $\bar{r}$ and $\bar{z}$. In doing this the integration is greatly simplified if the sample has been positioned so that the derivatives of the energy are slowly varying functions of $\bar{r}$ and $\bar{z}$. If that is the case, then the coefficients C_i are constants with respect to the integrations. Hence the scattering from samples with complicated geometries may be determined.

When the sample is highly absorbing, in the aspects of geometrical spread, the analysis of the situation is somewhat simplified in that the beam of x-rays does penetrate the sample, and the sample does not subtend many contour lines. When the sample is optically thin, we do not have to consider beam-attenuation effects. However, when we are in the intermediate region, attenuation effects must not be taken lightly since the effects of attenuation include not only loss of intensity but also a change in the shape of the distribution. One suggestion is to divide the sample into the segments that follow the contours of constant scattering energy followed by integration along each contour, which involves an integration only along either $\bar{r}$ or $\bar{z}$. Again, if the sample has been positioned properly, the coefficients C_i are constant with respect to the integration, so the integration is the length of the subtended arc of the contour weighted by the attenuation.

Regardless of the position of our effective sample (rectangular in shape) along a contour, there is a preferred orientation of the sample. The surface (longest dimension) of the sample should be placed tangent to the contour. This means (1) when $\bar{z}=0.5$ the sample surface should be placed parallel to the source-detector axis, (2) when $\bar{z}<0.5$ the surface should be "tilted" towards the detector, and (3) when $\bar{z}>0.5$ the sample should be tilted towards the source.

V. CONCLUSIONS

We have developed a mathematical method for determining the geometrical spread in the Compton-scattered x-ray energy distribution. The method presented is based on the realization that in a scattering geometry we have surfaces of constant scattering angle and hence surfaces of constant scattering energy that are toroidal in shape. With this realization, it is relatively easy to establish equations for determining the spread in energy caused by the geometry of a measuring system. In assessing a system, or when trying to optimize a system, it is important for the experimenter to realize that it is the gradients in the energy contours that exist within the scattering volume that actually determines the magnitude of the geometrical effects. This is important in cases, not uncommon in medical physics, where the sample itself is large and optically thin.

ACKNOWLEDGMENTS

The authors would like to thank Dr. M. Meron for reviewing this manuscript. This research was supported in part (A.L.H.) by the Processes and Techniques Branch, Division of Chemical Sciences, Office of Basic Energy Sciences, U. S. Department of Energy, under Contract No. DE-AC02-76CH00016 and through North Atlantic Treaty Organization Grant No. 0456/88.

[1]A. L. Huddleston and D. Bhaduri, Phys. Med. Biol. **24**, 310 (1979).

[2]C. E. Webber and T. J. Kennett, Phys. Med. Biol. **21**, 760 (1976).

[3]G. E. Gigante, in *Nuclear Analytical Techniques in Medicine*, edited by R. Cesareo (Elsevier, Amsterdam, 1988), Chap. 5.

[4]R. S. Holt, M. J. Cooper, and D. F. Jackson, Nucl. Instrum. Methods **221**, 98 (1984).

[5]A. L. Hanson, H. W. Kraner, K. W. Jones, B. M. Gordon, R. E. Mills, and J. R. Chen, IEEE Trans. Nucl. Sci. **NS - 30**, 1339 (1983).

[6]I. K. MacKenzie, B. G. Williams, T. G. Sparrow, and J. R. Stone, Proc. R. Soc. London, Ser. A **389**, 405 (1985).

[7]P. Pattison and J. R. Schneider, Nuc. Instrum. Methods **158**, 145 (1979).

[8]G. Matscheko and R. Ribberfors, Phys. Med. Bio. **32**, 577 (1987).

[9]G. Matscheko and G. A. Carlsson, Phys. Med. Bio. **34**, 185

(1989).
[10]G. A. Carlsson, C. A. Carlsson, K.-F Berggren, and R. Ribberfors, Med. Phys. **9**, 868 (1982).
[11]R. Ribberfors and K.-F Berggren, Phys. Rev. A **26**, 3325 (1982).
[12]A. L. Hanson, G. E. Gigante, and M. Meron, Phys. Rev. Lett. **61** 135 (1988).
[13]A. M. Ghose, European Community Joint Research Centre, Ispra, Italy, Report No. EUR-10968, 1987 (unpublished).
[14]J. Chomilier, G. Loupias, and J. Felsteiner, Nucl. Instrum. Methods **A235**, 603 (1984).
[15]G. Loupias, J. Chomilier, and S. Rabii, Ann. Phys. (Paris) Colloq. **11**, C2-65 (1986).